RADIOMETRIC AERIAL TRIANGULATION APPROACH. A CASE STUDY FOR THE Z/I DMC.

José González-Piqueras[1], David Hernández[1], Beatriz Felipe[1], Magali Odi[1], Soledad Belmar[1], Guillermo Villa[2] and Emilio Domenech[2]

[1]Remote Sensing and GIS Group
Regional Development Institute (IDR)
02071 Campus of Albacete (Spain)
Tf: 00 34 967599285
email: Jose.Gonzalez@uclm.es, David.Hernandez@uclm.es, Beatriz.Felipe@uclm.es, Soledad.Belmar@uclm.es, magaliodi@gmail.com

[2]Sub-Department of Territory Monitoring
National Geographic Institute of Spain (I.G.N.)
C/ General Ibañez Íbero, 3
E-28003 Madrid (Spain)
email: gmvilla@fomento.es, edomenech@fomento.es

KEY WORDS: Aerial Orthophotography, Radiometric correction, Radiometric Aerial triangulation, BRDF

ABSTRACT:

An important feature passing from the film to digital imaging is their high radiometric potential. Previous studies show limitations in the quantitative use of the image radiometry and the accurate radiometry is nowadays a new issue in photogrammetric processes. It is a well-stablished issue in remote sensing systems but can not be automatically implemented in photogrammetric processing lines due to the special features of photogrammetric data acquisition. An accurate radiometric calibration takes into account factors related to the system (sensor and data post-processing), photogrammetric network, the conditions of the acquisition (system settings, atmosphere, illumination and observation) and the target (anisotropy, topography, adjacent objects,...). This work is about the study and improvement of the thecniques used for the atmospheric and anisotropy correction of aerial images. For this purpose the atmospheric correction agorithms used in remote sensing have been adapted for an in-flight calibration of the camera with field spectral measurements during the 2009 year. The coefficients were obtained trough a least square minimization using the location of the spectral field points within the overlapping image areas. The method can be called as radiometric aerial triangulation similar to a geometric aerial triangulation. The radiative transfer equation was inverted to provide the image reflectance at field level over the 2006 dataset in Albacete (Spain). In a parallel way a semi-emprical kernel-driven model was applied to the image digital numbers in order to homogeneize the anisotropy in the BRDF over large observing angles. Atmospheric correction show at field image reflectance values within the range of typical measured values due to favorable and stable atmospheric conditions. The BRDF correction introduces an evident homogeneization of the image DN, providing the best results the geometric kernel Lidense without distinguishing between cover types.

1 INTRODUCTION

The systematic planning and the increasing radiometric quality of aerial images introduces a new tool for quantitative remote sensing (Honkavaara et al., 2009). Photogrammetry projects provide thousand of images database along different days over different countries. A premise in the photogrammetry projects is a high productivity and factors affecting the radiometry such as the illumination and observation conditions are no taken into account. Different studies about the radiometry potential of the aerial photography show important limitations in their quantitative use due to a poor description of the calibration of the sensor and the information process. Users in general and public institutions in particular that supports the national territory observation plans, are interested about the use of the radiometric information in the high spatial resolution photogrammetric images. The transition from the analogical to the digital image make the spectral and the spatial features of the aerial photography relevant data for their use in environmental models, orthophoto production, agricultural, forestry, remote sensing applications for monitoring natural resources, hydrologic models, etc... Nowadays the radiometric aspects are going to be taken into account in the photogrammetric process chains focusing in producing a repetitive image collection, maintaining a rigorous geometry and stereoscopy under large observation angles.

The objective of the radiometric correction in remote sensing is to remove the effects (environmental, target and sensor) that do not allow a quantitative and rigorous study of the information contained in the images. The reflectance at field level in absolute or relative terms is in most of cases the main physical magnitude provided in the radiometric corrections. In contrast, for visual analysis the objective is to reproduce the natural colors. The first step in a radiometric correction process is to apply the instrument corrections (geometric and radiometric) using the sensor calibration, the image or the flight stored information. The radiometric process comprises two phases, the first is the radiance that leaves the target and enters into the sensor, the second is the transformation of the energy flux to digital numbers (DN). During all of the radiation transfer process, the illumination and the atmosphere properties and their changes introduces variations in the signal. The absolute radiometric calibration determines for each channel the models and parameters for converting the DN to radiances [W m^{-2} nm^{-1} sr^{-1}], normally based on linear models for the CCD sensors. The relative radiometric calibration is a normalization of the image values obtained when the focal plane of the sensor is irradiated under an uniform field. The different methods of radiometric calibration can be classified in laboratory, in flight, over test plots (vicarious) and autocalibration. The vicarious methods determine the calibration of the sensor in the flight conditions using targets during the

image acquisition, typically artificial or natural surfaces, as soils, asphalt, etc... To determine accurately the radiation entering the sensor the vicarious methods require either accurate information on atmospheric conditions and object reflectance (reflectance-based method), or simultaneous determination of the at-sensor radiance by a calibrated radiometer (Markelin et al., 2008, Martínez et al., 2007). Within this objective recently, several field campaigns were carried out flying hyperspectral sensors, field spectra acquisition and atmosphere characterization in coincidence to the photogrammetric flight (Martínez and Arbiol, 2009). An adequate laboratory calibration allows to obtain an accurate sensor response under a wide range of conditions. The laboratory calibration could be the only radiometric calibration method needed if ideal conditions are met (accurate, stable sensor and rigorous calibration facility),

A key factor is to remove the noise introduced by the presence of the atmosphere. The radiative transfer code provides a physical solution of the radiative transfer equation (Liang, 2004), and a well-know are the 6S (Vermote et al., 1997) and MODTRAN (Berk et al., 1999). These codes have been implemented in commercial software that allow an automatic atmospheric correction as ATCOR4 (Richter, 2009) or FLAASH (Cooley et al., 2002). The inversion of these radiative transfer codes provides the directional reflectance at-field from the radiance at sensor level calibrated radiometrically. The atmospheric corrections applied in aerial photography were empirical (Haest et al., 2009), using the radiative transfer code (Chandelier and Martinoty, 2009) and obtaining the atmospheric parameters by means of coincident in time hyperspectral images (Martínez et al., 2007). The photogrammetric flights introduce repetitive acquisitions with overlapping areas that ranges from 20 - 80 %. An important improvement can be the use of these overlapping areas under different environment, illumination and observation conditions for obtaining coherent radiometric calibration of the aerial images.

The use of the aerial imagery under large observation angles, such as for obtaining uniform mosaics, requires an appropriate correction of the anisotropy introduced by the bidirectional reflectance distribution function (BRDF), know as the target materials' view angle and wavelength dependent reflectance function. Different physical (i. e analytical) and empirical BRDF models haven proposed for correcting the anisotropy of reflectance (Verger et al., 2005, Liang, 2004). Physical models are the most complex, and since they normally have nonlinear properties, inversion requires many highly accurate observations or a priori knowledge, and has a very high computational load. In the last few years, the semi-empiriral kernel driven models have gained significant attention to normalize remote sensing and photogrammetric data (Haest et al., 2009, Wu, 2006). These kernel-driven methods are based on linear combinations of so-called kernels. Each of these kernels is an angular-dependent function that accounts for part of the angular reflectance behavior.

Within the Spanish National Orthophoto Plan (PNOA, *Plan Nacional de Ortofotografía Aérea*) for the year 2009, a field campaign was carried out using surfaces that can be considered invariants taking into account previous studies (Haest et al., 2009, Martínez and Arbiol, 2009, Markelin et al., 2008) for correcting the 2006 and 2009 DMC images dataset. For this purpose, two corrections were applied to the 2006 dataset, atmospheric and BRDF. The calibration coefficients were obtained using the field measured reflectance in points located in the overlapping areas between the images. This technique is similar to the geometric aerial triangulation and can be understood as a radiometric aerial triangulation. The radiative transfer equation was inverted for

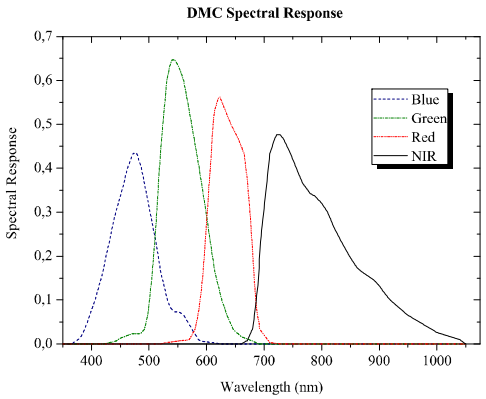

Figure 1: Spectral response of the DMC (www.intergraph.com)

obtaining the reflectance images at field level. In a parallel way the anisotropy correction was applied to the entire set of images selected over the DN.

2 MATERIAL AND METHODS

2.1 The DMC Camera

The Z/I Digital Metric Camera (DMC) simultaneously captures a high resolution panchromatic image of 13,824 x 7,680 pixels and four multispectral images of 3,072 x 2,048 pixels in the red (R), green (G), blue (B) and nearinfrared (NIR) (Figure 1). The lower resolution multi-spectral images in the RGB and NIR are acquired by four nadir looking camera heads with a focal length of 25 mm (www.intergraph.com). The DMC instantaneous field of view (IFOV) or is 69.3^o across strip and 42^o along strip with a radiometric resolution of 12 bit. The high resolution multispectral image was obtained fusing the panchromatic and the multispectral images. The DMC camera has a high radiometric performace but the calibration report does not provide an absolute calibration to obtain absolutely physical measurements in radiance units.

The PNOA for the year 2006 acquired the original 12 bit images at 45 cm GSD, with an overlapping area of 65 % along strip and 25 % across strip.The LRC images were used for the atmospheric correction in order to guarantee the linearity of the camera in the conversion from DN to radiances avoiding the gamma, Fritsh-Carlson, lineal transformation and pan-sharpening.

2.2 The Field Reflectance Data

The field campaign was set coincident in time to the PNOA 2009 flight on July 26th. The field measurements allow an absolute radiometric calibration of the 2009 flight and a post-calibration of the 2006 orthophotography. The ASD FieldSpec 3 (www.asd.com) spectroradiometer were used for the measurements of reflectance within a range of 350-2500 nm with an acquisition time of 0,1 s. It incorporates a bare fiber with an IFOV of 25^o, observing the target at 1 m over the nadir. The GPS Leica 1200 used for the field measurements guarantees the precise location of the target. To minimize the error during the field measurements the observing geometry (North to South) was constant during all the acquisitions avoiding shadows and user influence. The atmosphere was clear without clouds under direct solar radiation. The incident radiation over the

reference Spectralon panel was acquired prior to each target for avoiding errors in the illumination changes between the spectral measurements A minimum set of 6 samples were acquired for each target .The field measurements were made within the area covered in the set of 6 images selected (left image composition on Figure 3) and resumed in Table 1.

Target	Number of Pointsr
Sandy Soil	1
Grass	26
Bare Soil	16
Road	2
Asphalt	4
Water	2
Coloured canvas	1

Table 1: Surfaces used in the field radiometric measurements.

2.3 The atmospheric correction

The signal that reaches the aerial sensor is composed by the path radiance ($L_{path,}$ including the photons scattered by the atmosphere without contacting the target), the radiance reflected by the target $L_{ref,}$ and the radiance reflected by the surrounding area that is scattered by the atmosphere and entered into the sensor $L_{adj.}$. The atmospheric correction removes the scattered terms in the radiation transfer equation. So the wavelength dependant radiance that reaches the sensor (L_λ) comprises the terms:

$$L_\lambda = L_p + L_{ref} + L_{adj} \tag{1}$$

The digital number (DN_λ) registered by the sensor can be linearly related to the incoming radiance, establishing the relationship $L_\lambda = C_{0\lambda} + C_{1\lambda} \cdot DN_\lambda$. The $C_{0\lambda}$ and $C_{1\lambda}$ are the calibration coefficients of the sensor. Without taking into account the adjacency term in the equation 1, a first approximation to the target reflectance (ρ_t) for flat terrain can be obtained as:

$$L_\lambda = \frac{\mu_s \cdot E_s}{\pi} \cdot \left[\rho_a + \frac{\rho_t}{1 - s \cdot \rho_t} \tau_g \tau(\theta_s) \tau(\theta_v)\right] \tag{2}$$

The factor $\mu_s = \cos\theta_s$, is referred to the sun zenith angle. E_s is the solar flux at the top of the atmosphere, τ_g is the global transmittance, ρ_a is the atmosphere intrinsic reflectance, $\tau(\theta_s)$ and $\tau(\theta_v)$ are the total transmittance from sun to target and from target to sensor respectively and s is the albedo.

The sun zenith and azimuth angle were calculated applying the Solar Position Algorithm (SPA) (Reda and Andreas, 2008) from the flight parameters. The terms E_s, τ_g, ρ_a, $\tau(\theta_s)$, $\tau(\theta_v)$ and s of the equation 2 have been reported generating the atmospheric profiles at 5 km flight altitude using the radiative transfer code 6S (Veromote et al., 1997) for a visibility of 30 km, water vapor content of 2.0 g/cm^2 and rural aerosol model.

The calibration coefficients have been obtained using the field spectral measurements solving the m equations corresponding the total n radiometric points measured in each image. In order to minimize the rough error introduced due to the not coincidence in time for the field measurements and flight, a minimization method was applied.

The inverse method, using the calibration coefficients obtained, was applied to the images for obtaining the atmospherically corrected reflectance taking into account the variability in the factor $\tau(\theta_v)$. From an operational point of view, a unique value of $\tau(\theta_s)$, τ_g, μ_s, ρ_a, and s were used for each image.

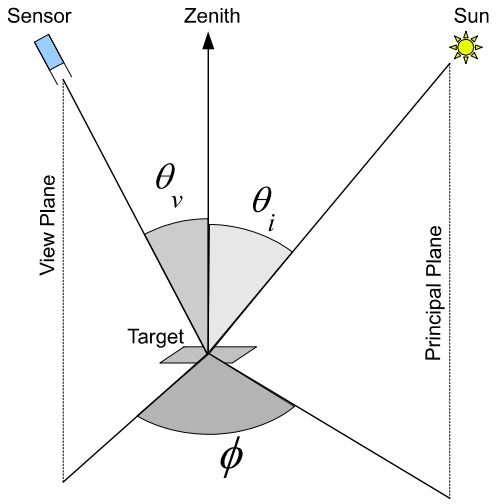

Figure 2: Graphic description of zenith and azimuth angles.

2.4 The BRDF correction

The differences in the target reflectance when it is observed from different illumination and observation configuration has been normalized from different authors (Wu, 2006, Chandelier and Martinoty, 2009). In particular, for the aerial cameras with a wide IFOV it can be an important factor, and can be corrected . The kernel-driven model considers the spectral reflectance in terms of its angular behavior as:

$$\rho\left(\theta_i, \theta_v, \phi; \lambda\right) = k_0\left(\lambda\right) + k_1\left(\lambda\right) f_1\left(\theta_i, \theta_v, \phi\right) + k_2\left(\lambda\right) f_2\left(\theta_i, \theta_v, \phi\right) \tag{3}$$

ρ surface reflectance,

θ_s solar zenith angle

θ_v observation zenith angle

ϕ azimuth angle between the principal and the observation plane.

λ wavelength

f_1 geometric kernel

f_2 volumetric kernel

k_0, k_1, k_2 weight factors for the isotropic, geometric and volumetric kernel respectively.

The coefficients k_0, k_1, k_2 are calculated for each image, selecting the radiometric tie points by a systematic random sample in the overlapping area between images. A number of m equations have been generated for n tie points. For a simple case of a point located in two images, the equation system can be expressed as:

$$\begin{aligned} v_1 &= k_{01} + k_{11} f_{11} + k_{21} f_{21} - g_1 \\ v_2 &= k_{02} + k_{12} f_{12} + k_{22} f_{22} - g_1 \\ v_3 &= k_{01} + k_{11} f_1 + k_{21} f_2 - k_{02} + k_{12} f_1 + k_{22} f_2 - (g_1 - g_2) \end{aligned} \tag{4}$$

where the coefficients k_{i1} and k_{i2} are the unknown coefficients in the first and second image respectively. g_1 and g_2 are the pixel value in each image and v_i $(i = 1, 2, 3)$ are the residuals.

The equation system and the weight coefficients (w_i, $i = 1, 2, 3$) are solved by the minimum least square method.

The solution of the system is applied to the entire image using the equation:

$$ND_c = ND\frac{k_{01} + k_{11}f_{11}^z + k_{21}f_{21}^z}{k_{01} + k_{11}f_{11} + k_{21}f_{21}} \quad (5)$$

where ND and ND_c are the original and corrected image values respectively. The f_{11}^z and f_{21}^z are the kernels calculated for a vertical observation, $\theta_v = 0$. The BRDF correction in this work was applied over the set of 8 bit image, with different geometric and volumetric kernel combinations.

3 RESULTS

3.1 BRDF correction

The kernel driven correction was applied without distinguishing between different surfaces, obtaining the best results with the Lidense kernel for all the spectral bands. The application of the different (geometric and volumetric) kernel combinations show a homogenization of the images and visual differences between the different geometric kernels were observed. A mosaic of six images corrected by the BRDF using the Lidense geometric kernel in DN is shown on figure 3 Minor visual differences were observed when applying the volumetric kernel that introduces a second order correction. The blue and nir bands suffered a minor normalization of the anisotropy, and it can be due to a major influence the atmospheric effects.

Figure 3: Original Orthoimage (left) and homogeneized (right) applying the Lidense geometric kernel.

3.2 Atmospheric correction

In the figure 4 is shown the original image on the left and the atmospherically corrected reflectance on the right. An important reduction of the blue-to-white visual effect over the true color image due to haze can be observed.

Several representative field spectra (lines) are shown in figure 5 compared to the atmospherically corrected reflectance images (marks) for similar surfaces in the area. The figure shows similar reflectance results in the visible bands but appreciable differences in the nir for vegetation. The reflectance of vegetation cover is very sensitive in the nir due to changes in the crop architecture and this difference indicates the variability of grass. The differences observed between the reflectance in the other surfaces are due to factors included in the calibration coefficients such as deviation of atmosphere components than used for determining the atmospheric profiles, integration time, aperture or directional effects.

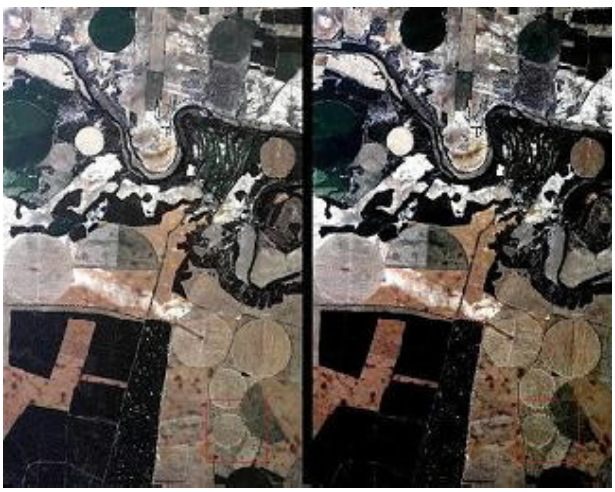

Figure 4: Original DN image (left) and atmospherically corrected reflectance (right).

4 CONCLUSIONS

The radiometric calibration of the aerial images comprises the atmospheric correction and, taking into account the large view angles of the cameras, the anisotropy correction. The two correction methods have been adapted and applied for the DMC images of the year 2006. By one side the atmospheric correction using invariant field data acquired on the year 2009, and by other side the radiometric homogenization of the DN were applied.

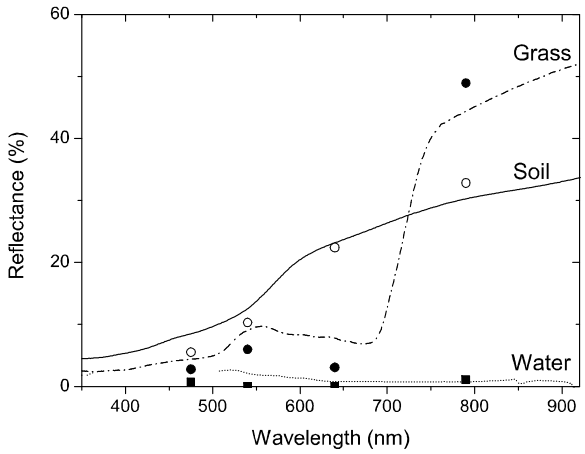

Figure 5: Comparison of representative field measurements (lines) with the image atmospherically corrected reflectance values for soil (o), water (■) and grass (●)

The atmospheric correction was set using standard atmospheric profiles for obtaining the calibration coefficients of the camera. The exposition time and the aperture of the camera was automatic and the coefficients obtained could no be applied to other images than used. Despite this factor, a first quantitative analysis of the results show that the reflectance images are within the range and the slope of the field spectra in the study area (vegetation, soil, asphalt) in the visible and nir range.

The BRDF correction over the DN in the camera show promising results providing a visual homogenization of the images. The best correction was obtained applying the geometric Lidense kernel-driven without distinguishing the cover type. The results obtained for a unique cover type is an important advantage of the method for reducing the computation load, but validation data are needed for a quantitative study of the results about the limitation of the method. This work shows the possibility of calibrate the yet existing and future time digital image series for merging image data of different sensors and their future use for both photogrammetry and environmental applications.

ACKNOWLEDGEMENTS

This work was carried out within the project "Joint project for the radiometric aerial triangulation of aerial images" (Contract number.UCTR080230) supported by the National Geographic Institute of Spain (IGN), in collaboration to Tragsatec and the IGN. The authors thanks to the Cartographic Institute of Catalonia (ICC) for its advice and the material used in the field campaign.

REFERENCES

Berk, A., Anderson, G., Bernstein, L., Acharya, P., Dothe, H., Matthew, M., Adler-Golden, S., Chetwynd Jr., J., Richtsmeier, S., Pukall, B., Allred, C., Jeong, L. and Hoke, M., 1999. Modtran4 radiative transfer modeling for atmospheric correction. Vol. 3756, pp. 348–353. cited By (since 1996) 59.

Chandelier, L. and Martinoty, G., 2009. A radiometric aerial triangulation for the equalization of digital aerial images and orthoimages. Photogrammetric Engineering and Remote Sensing 75(2), pp. 193–200.

Cooley, T., Anderson, G., Felde, G., Hoke, M., Ratkowski, A., Chetwynd, J., Gardner, J., Adler-Golden, S., Matthew, M., Berk, A., Bernstein, L., Acharya, P., Miller, D. and Lewis, P., 2002. Flaash, a modtran4-based atmospheric correction algorithm, its applications and validation. Vol. 3, pp. 1414–1418. cited By (since 1996) 6.

Haest, B., Biesemans, J., Horsten, W., Everaerts, J., Van Camp, N. and Van Valckenborgh, J., 2009. Radiometric calibration of digital photogrammetric camera image data. In: ASPRS 2009 Anual Conference, Baltimore, Maryland.

Honkavaara, E., Arbiol, R., Markelin, L., Martínez, L., Cramer, M., Bovet, S., Chandelier, L., Ilves, R., Klonus, S., Marshal, P., Schlapfer, D., Tabor, M., Thom, C. and Veje, N., 2009. Digital airborne photogrammetry: A new tool for quantitative remote sensing?. a state-of-the-art review on radiometric aspects of digital photogrammetric images. Remote Sensing 1(3), pp. 577–605.

Liang, S., 2004. Quantitative Remote Sensing of Land Surfaces. Wiley-Interscience.

Markelin, L., Honkavaara, E., Peltoniemi, J., Ahokas, E., Kuittinen, R., Hyyppaï, J., Suomalainen, J. and Kukko, A., 2008. Radiometric calibration and characterization of large-format digital photogrammetric sensors in a test field. Photogrammetric Engineering and Remote Sensing 74(12), pp. 1487–1500.

Martínez, L. and Arbiol, R., 2009. Banyoles 2008 campaign dataset. Technical Report.

Martínez, L., Arbiol, R., Palá, V. and Pérez, F., 2007. Digital metric camera radiometric and colorimetric calibration with simultaneous casi imagery to a cie standard observer based colour space. In: Geoscience and Remote Sensing Symposium, 2007. IGARSS 2007. IEEE International.

Richter, R., 2009. Atmospheric / topographic correction for airborne imagery (atcor-4 user guide, version 5.0, january 2009). Technical report, DLR German Aerospace Center.

Verger, A., Camacho-de Coca, F. and Meliá, J., 2005. Revisión de los modelos paramétricos de brdf. Revista de Teledetección 23, pp. 65–80.

Vermote, E., Tanré, D., Deuzé, J., Herman, M. and Moncrette, J., 1997. Second simulation of the satellite signal in the solar spectrum. IEEE Transactions on Geoscience and Remote Sensing 35, pp. 675–686.

Veromote, E., Tanré, D., Deuzé, J., Herman, M. and Morcrette, J., 1997. Second simulation of the sattelite signal in the solar spectrum (6s) (user guide version 2). Technical report, NASA.

Wu, X., 2006. Radiometric calibration of aerial digital imagery. In: CSIRO Mathematical and Information Sciences.